Close-coupled model of Feshbach resonances in ultracold ^{3}He* and ^{4}He* atomic collisions

T. M. F. Hirsch,* D. G. Cocks, and S. S. Hodgman
Research School of Physics, Australian National University, Canberra 0200, Australia

(Received 27 May 2021; accepted 2 September 2021; published 20 September 2021)

Helium atoms in the metastable $2\,^3S_1$ state (He*) have unique advantages for ultracold atomic experiments. However, there is no known accessible Feshbach resonance in He* which could be used to manipulate the scattering length and hence unlock several new experimental possibilities. Previous experimental and theoretical studies for He* have produced contradictory results. We aimed to resolve this discrepancy with a theoretical search for Feshbach resonances, using a close-coupled model of He* collisions in the presence of an external magnetic field. Several resonances were detected and the existing literature discrepancy was resolved. Although none of the resonances identified are readily experimentally usable, an interesting non-Feshbach scattering length variation with magnetic field was observed in heteronuclear collisions, at field strengths that are experimentally accessible.

DOI: 10.1103/PhysRevA.104.033317

I. INTRODUCTION

Ultracold atomic gases are a unique experimental platform for the study of atomic and molecular physics and quantum mechanics. The simplicity, isolation, and fewer degrees of freedom offered by such systems allow exciting experiments to be performed such as Bose-Einstein condensation [1] and the trapping of atoms in periodic optical lattices [2]. One feature of ultracold gases is that the collisions between atoms are accurately described by a single parameter: the *s*-wave scattering length. Feshbach resonances allow the tuning of the scattering length, typically via the application of an external magnetic field. Suitable resonances have facilitated experiments such as exploring quantum phase transitions [3], superfluidity regimes [4], realizing negative temperature states [5], or "Bose-nova" condensate collapse [6].

Metastable helium (He*) atoms possess unique advantages in ultracold experiments as the large internal energies of these atoms allow charged plate detectors to achieve individual atom detection with relatively high spatial and temporal resolution [7]. He* atoms are trapped in the $2\,^3S_1$ excited state of helium, which has a lifetime of 2.2 hours [8], longer than the timescale of typical ultracold experiments, and an internal energy of 19.8 eV [9], the largest of any metastable atom. These properties have facilitated unique experiments such as studies of Hanbury Brown–Twiss style matter wave interference [10], production and detection of Bell correlated atomic pairs [11,12], and ghost imaging [13]. Several extensions to these, as well as other proposed experiments for He*, would benefit from the use of a Feshbach resonance to tune the scattering length. These include controlling the rate of entanglement generating collisions [11,14], adjusting the two-body interaction parameter in many-body lattice experiments [15], and increasing the quantum depleted fraction of a BEC [16,17].

Unfortunately, He* experiments have been unable to use a Feshbach resonance, because it is unknown if an experimentally accessible Feshbach resonance exists in this state. There has been a single theoretical study of this problem [18] which used a perturbative treatment called the asymptotic bound state model. That study predicted multiple resonances over the different isotopic mixtures, albeit many were too narrow and/or required too high magnetic field strengths to be experimentally useful. However, an experimental search for the most promising of the predicted ^{4}He* resonances failed to observe it [19], suggesting further investigation is required.

In this paper we develop a nonperturbative, *ab initio* close coupled model of metastable helium atoms in the presence of a magnetic field. Our results resolve the discrepancy between the prior study and experiment: the resonance that was not seen in the experiment is broadened by ionization effects that were discounted in the perturbative treatment. We identify several other resonances, as well as interesting non-Feshbach-resonance magnetic field dependence.

II. METHODS

This approach mostly follows that of [20], extending the method to include the Zeeman interaction. Briefly, we write the scattering wave function of the colliding atoms in a basis of states called channels, and use that decomposition to solve the scattering Schrödinger equation. Fitting to the large-distance solution yields a scattering matrix containing information such as cross sections. The model was written in the JULIA programming language [21] using the DIFFERENTIALEQUATIONS package [22].

A. Hamiltonian

The scattering of two metastable helium atoms in an external magnetic field is governed by the Hamiltonian

$$\hat{H} = \hat{T} + \hat{H}_{\rm el} + \hat{H}_{\rm rot} + \hat{H}_{\rm sd} + \hat{H}_{\rm zee} + \hat{H}_{\rm hfs}, \qquad (1)$$

*Present address: School of Mathematics and Physics, The University of Queensland, St. Lucia 4072, Australia; timothy.hirsch@uq.edu.au

where

$$\hat{T} = \frac{-\hbar^2}{2\mu}\frac{1}{R^2}\frac{\partial}{\partial R}\left(R^2\frac{\partial}{\partial R}\right) \tag{2}$$

is the kinetic term and

$$\hat{H}_{\rm rot} = \frac{\hat{l}^2}{2\mu R^2} \tag{3}$$

is the centripetal operator effective in spherical coordinates;

$$\hat{H}_{\rm el} = \hat{H}_1 + \hat{H}_2 + \hat{H}_{12} \tag{4}$$

is the electronic Hamiltonian, $\hat{H}_i$ representing the kinetic term for the electrons in atom i and $\hat{H}_{12}$ representing the Coulombic interaction between the two atoms;

$$\hat{H}_{sd} = -\frac{\xi}{\hbar^2 R^3}[3(\hat{\mathbf{S}}_1\cdot\hat{\mathbf{R}})(\hat{\mathbf{S}}_2\cdot\hat{\mathbf{R}}) - \hat{\mathbf{S}}_1\cdot\hat{\mathbf{S}}_2] \tag{5}$$

is the spin-dipole interaction between the magnetic dipole moments of the two atoms. In the above, $\hat{\mathbf{S}}_i$ is the spin operator for atom i, $\hat{\mathbf{R}}$ is the unit vector along the internuclear axis, and

$$\xi = \alpha^2\left(\frac{\mu_e}{\mu_B}\right)^2 E_{\rm h} a_0^3. \tag{6}$$

Here α is the fine structure constant, μ_e and μ_B are respectively the electron magnetic moment and Bohr magneton, $1E_{\rm h} \approx 27.2$ eV is a hartree, and $1a_0 \approx 0.529$ Å is a Bohr radius.

$$\hat{H}_{\rm zee} = -\frac{g_s\mu_B}{\hbar}\mathbf{B}\cdot(\mathbf{S}_1 + \mathbf{S}_2) \tag{7}$$

is the Zeeman interaction of the atomic spins in the magnetic field, where $g_s \approx 2$ is the electronic spin g factor.

Finally, $\hat{H}_{\rm hfs}$ is the hyperfine structure term which is only for ^{3}He* atoms. The form of $\hat{H}_{\rm hfs}$ is given below in Sec. II D.

B. Coupled channels approach

We use the coupled channel formalism, which expands the scattering wave function $|\Psi\rangle$ into a basis of molecular states $|a\rangle$ using radial functions $G_a(R)$:

$$|\Psi(R)\rangle = \sum\frac{1}{R}G_a(R)|a\rangle. \tag{8}$$

The molecular states, called channels, are eigenstates of the system Hamiltonian at asymptotically large separation distances. We label them open or closed if the eigenvalues of

$$\hat{H}_{\rm asymp} = \hat{H}_1 + \hat{H}_2 + \hat{H}_{\rm zee} + \hat{H}_{\rm hfs} \tag{9}$$

are greater or lesser, respectively, than the total energy (i.e., closed channels are energetically forbidden at large separation distances). We also invoke the Born-Oppenheimer approximation, assuming that the channels have only a parametric dependence on the internuclear separation R. This means we assume $\partial|a\rangle/\partial R = \partial^2|a\rangle/\partial R^2 = 0$. From this approximation the time-independent Schrödinger equation,

$$\hat{H}|\Psi\rangle = E|\Psi\rangle, \tag{10}$$

can be manipulated to yield the multichannel equations for the radial wave functions:

$$\sum_a\left[\frac{-\hbar^2}{2\mu}\frac{d^2}{dR^2}\delta_{a'a} + V_{a'a}(R) - E\delta_{a'a}\right]G_a(R) = 0, \tag{11}$$

where $V_{a'a}(R) = \langle a'|\hat{V}(R)|a\rangle$ and $\hat{V} = \hat{H} - \hat{T}$.

C. Basis

It is difficult to directly write down a basis that simultaneously diagonalizes the Zeeman and hyperfine interactions, which are both present at large separation distances. Instead we perform the calculation in a basis whose elements can be easily listed and find the eigenstates by numerically diagonalizing the long-distance Hamiltonian.

The easily enumerated basis we use is the hyperfine basis:

$$|a\rangle \equiv |\alpha\beta\, l m_l\rangle \equiv |(S_\alpha i_\alpha f_\alpha m_{f_\alpha})(S_\beta i_\beta f_\beta m_{f_\beta})\, l m_l\rangle. \tag{12}$$

Here α and β list the magnetic spin numbers for atoms α and β, with the electronic and nuclear spins of each atom coupled as $\mathbf{S}_j + \mathbf{i}_j = \mathbf{f}_j$. $l = 0, 1, 2, \ldots$ is the rotational angular momentum of the two-atom system.

In the case of homonuclear collisions these basis states must be symmetrized to obey the fermionic and bosonic symmetry of ^{3}He*-^{3}He* and ^{4}He*-^{4}He* respectively [23]. We form symmetrized states $|\{\alpha\beta\}\, l m_l\rangle$ as linear combinations [20]:

$$|\{\alpha\beta\}\, l m_l\rangle = \frac{|\alpha\beta\rangle + (-1)^{i_\alpha+i_\beta+l}|\beta\alpha\rangle}{\sqrt{2(1+\delta_{\alpha\beta})}} \otimes |l m_l\rangle. \tag{13}$$

In the case of ^{3}He*-^{4}He* collisions we use the unsymmetrized $|\alpha\beta\, l m_l\rangle$ states.

D. Matrix elements

When integrating the multichannel equations (11) we must calculate the matrix elements $V_{aa'}(R)$.

The rotational interaction has the simplest matrix element:

$$\langle a'|\hat{H}_{\rm rot}|a\rangle = \delta_{a,a'}\frac{l(l+1)\hbar^2}{2\mu R^2}. \tag{14}$$

The matrix elements for $\hat{H}_{\rm el}$, $\hat{H}_{\rm zee}$, and $\hat{H}_{\rm sd}$ are evaluated by changing into the basis associated with the coupling scheme $\mathbf{S}_\alpha + \mathbf{S}_\beta = \mathbf{S}$, using the expansion in terms of Clebsch-Gordan coefficients:

$$|\alpha\beta\rangle = \sum_{\substack{m_S^\alpha \\ m_i^\alpha}}\sum_{\substack{m_S^\beta \\ m_i^\beta}}\sum_{\substack{S \\ m_S}} C^{S_\alpha i_\alpha f}_{m_S^\alpha m_i^\alpha m_f^\alpha} C^{S_\beta i_\beta f_\beta}_{m_S^\beta m_i^\beta m_f^\beta} C^{S_\alpha S_\beta S}_{m_S^\alpha m_S^\beta m_S} \times \left|(S_\alpha S_\beta S m_S)\left(i_\alpha m_i^\alpha i_\beta m_i^\beta\right)\right\rangle. \tag{15}$$

In this basis $\hat{H}_{\rm el}$ is diagonal:

$$\hat{H}_{\rm el}|S m_S\rangle = {}^{2S+1}V_\Sigma(R)|S m_S\rangle. \tag{16}$$

The quintet Born-Oppenheimer $^5\Sigma_g^+$ potential is taken as the analytic form described by Przybytek and Jeziorski [24]. The singlet $^1\Sigma_g^+$ and triplet $^3\Sigma_u^+$ potentials are interpolated from the tabulated values of Müller *et al.* [25] within the $3a_0 < R < 14a_0$ range where those values are given, and fitted to the

${}^5\Sigma_g^+$ potential at larger distances. Following the method of [20], this fitting is done using an exponentially decaying exchange term: ${}^{1,3}V_\Sigma(R > 14a_0) = {}^5V_\Sigma(R) - A_{1,3}\exp(-\beta_{1,3}R)$, where $A_1 = 5.9784$, $\beta_1 = 0.7367$, $A_3 = 1.7980$, and $\beta_3 = 0.6578$.

We write the spin-dipole as the product of two second-rank irreducible tensors $\hat{H}_{\rm sd} = V_p(R)\mathbf{T}^2 \cdot \mathbf{C}^2$, where $V_p(R) = b/R^3$ and $b = -\sqrt{6}\xi$ [26]. This gives the matrix elements as

$$\langle a'|\hat{H}_{\rm sd}|a\rangle = V_p(R)D_{aa'}. \tag{17}$$

The coupling coefficient is

$$\begin{aligned} D_{aa'} &= \delta_{m_{S'}+m_{l'},m_S+m_l}(-1)^{m'_S-m_S} \\ &\times C^{S\,2\,S'}_{m_{S'}\,m_{S'}-m_S\,m_{S'}} C^{l\,2\,l'}_{m_l\,m_{l'}-m_l\,m_{l'}} \\ &\times \langle S'_\alpha S'_\beta S'||\mathbf{T}^2||S_\alpha S_\beta S\rangle\langle l'||\mathbf{C}^2||l\rangle. \end{aligned} \tag{18}$$

The reduced matrix elements for the tensors $\mathbf{T}^2$ and $\mathbf{C}^2$ are

$$\begin{aligned} \langle S'_\alpha S'_\beta S'||\mathbf{T}^2||S_\alpha S_\beta S\rangle &= \delta_{S_\alpha,S'_\alpha}\delta_{S_\beta,S'_\beta} \\ &\times \sqrt{S_\alpha(S_\alpha+1)S_\beta(S_\beta+1)} \\ &\times \sqrt{5(2S+1)(2S_\alpha+1)(2S_\beta+1)} \\ &\times \begin{Bmatrix} S_\alpha & S_\beta & S \\ 1 & 1 & 2 \\ S_\alpha & S_\beta & S' \end{Bmatrix}, \end{aligned} \tag{19}$$

where the last factor is a Wigner 9-j coefficient, and

$$\langle l'||\mathbf{C}^2||l\rangle = \sqrt{\frac{2l+1}{2l'+1}}C^{l\,2\,l'}_{0\,0\,0}. \tag{20}$$

The matrix elements for the Zeeman interaction are simply

$$\langle S'\,m_{S'}|\hat{H}_{\rm zee}|S\,m_S\rangle = \delta_{S,S'}\delta_{m_S,m_{S'}}\frac{g_s\mu_B}{\hbar}Bm_S. \tag{21}$$

The relative difference between the electron spin g factor and the $2\,{}^3S_1$ g factor is of the order of 10^{-5} [27] and we therefore neglect it. We also neglect the contribution from nuclear spin because the nuclear magnetic moment is on the order of 10^3 smaller than the electronic magnetic moment [28].

$\hat{H}_{\rm hfs}$ is diagonal in this basis, with the matrix elements [29]

$$\langle a'|\hat{H}_{\rm hfs}|a\rangle = \delta_{a,a'}\left(E^{\rm hfs}_{i_\alpha,f_\alpha} + E^{\rm hfs}_{i_\beta,f_\beta}\right), \tag{22}$$

where

$$E^{\rm hfs}_{i,f} = \begin{cases} 1.519830\times10^{-7}\,E_{\rm h}, & i=\frac{1}{2}, f=\frac{3}{2}, \\ 0E_{\rm h} & \text{otherwise.} \end{cases} \tag{23}$$

To optimize the numerical integration routine we recognize that the nondiagonal interactions, $\hat{H}_{\rm el}$, $\hat{H}_{\rm sd}$, and $\hat{H}_{\rm zee}$, can be written separably as products of R-independent matrices and a scalar functions of R. For example, in the case of the electronic term,

$$\langle a|\hat{H}_{\rm el}(R)|a'\rangle = \sum_{S=0}^{2} C^{2S+1}_{aa'}V^{2S+1}(R), \tag{24}$$

where each $C^{2S+1}_{aa'}$ is a coupling coefficient. This separation of R-independent coupling terms can be written more generally as,

$$V_{aa'}(R) = \sum_k V^k_{aa'} \otimes f_k(R), \tag{25}$$

where $V^k_{aa'}$ would be a coupling coefficient and f_k a radial function. There are three different radial independent terms for $\hat{H}_{\rm el}$ (corresponding to the three values of $S = 0, 1, 2$) and one each for $\hat{H}_{\rm sd}$ and $\hat{H}_{\rm zee}$. We precalculate the radial-independent coupling coefficients for the nondiagonal interactions so that only the radial factors are repeatedly calculated.

Ionization processes were modeled through the use of complex potentials. In the case of singlet and triplet channels (the quintet channel is spin polarized, forbidding ionization) the potential was modified via the addition of an imaginary term:

$${}^{1,3}V(R) - \frac{i}{2}\,{}^{1,3}\Gamma(R), \tag{26}$$

where the autoionization width is

$${}^{1,3}\Gamma(R) = 0.3\exp\left(\frac{-R}{1.086}\right) \tag{27}$$

in units of $E_{\rm h}$, with R in units of a_0. This term comes from [30] and has been shown to be nearly identical to the ionization values described in Müller *et al.* [20,25].

E. Scattering matrices and cross sections

The scattering problem is constrained by inner and outer boundary conditions as $R \to 0$ and $R \to \infty$ respectively. All radial wave functions must vanish at the inner boundary where the potential diverges; additionally, all closed channel wave functions must vanish at the outer boundary. We define linearly independent initial conditions representing both sets of boundary conditions, and integrate those conditions to a single middle point. We then use a QR decomposition to find linear combinations of the boundary conditions that produce matching solutions at that point. These matched solutions satisfy both boundary conditions.

The matched solutions, evaluated at the outer boundary where the electronic and spin-dipole interactions can be safely neglected, are then fitted to spherical bessel functions, which represent the oscillatory asymptotic form of the scattering wave. Specifically, the solutions $\mathbf{F}(R)$ are matched to the form [31]

$$\mathbf{F}(R) \underset{R\to\infty}{\longrightarrow} \mathbf{J}(R)\mathbf{A} + \mathbf{N}(R)\mathbf{B}, \tag{28}$$

where $\mathbf{J}(R)$ and $\mathbf{N}(R)$ are diagonal matrices with the entries

$$\begin{aligned} J_{aa}(R) &= \sqrt{k_aR}\,j_{l_a}(k_aR), \\ N_{aa}(R) &= \sqrt{k_aR}\,n_{l_a}(k_aR). \end{aligned} \tag{29}$$

The matrices have one entry for each open channel a. Here k_a is the asymptotic wave number of channel a,

$$k_a = \frac{\sqrt{2\mu(E - V^\infty_{aa})}}{\hbar}, \tag{30}$$

where E is the total energy and $V^\infty_{aa} = \langle a|\hat{H}_{\rm zee} + \hat{H}_{\rm hfs}|a\rangle$. The wave number k_a characterises the kinetic energy available for scattering when the entrance channel is $|a\rangle$.

The fitted matrices **A** and **B** are used to define the reactance matrix $\mathbf{K} = \mathbf{B}\mathbf{A}^{-1}$, which then defines the scattering matrix:

$$\mathbf{S} = (\mathbf{I} + i\mathbf{K})(\mathbf{I} - i\mathbf{K})^{-1}. \tag{31}$$

Cross sections for scattering from one channel into another (including elastic scattering where the incoming and outgoing channels are identical) are defined from the scattering matrix:

$$\sigma(\gamma \to \gamma') = \frac{\pi}{k_\gamma^2} \sum_{l\, m_l\ \ l'\, m_l'} |T_{\gamma' l' m_l', \gamma l m_l}|^2, \tag{32}$$

where the transition matrix $\mathbf{T} = \mathbf{I} - \mathbf{S}$.

Similarly, the ionization cross sections are found from the nonunitarity of the scattering matrix:

$$\sigma(\gamma \to \mathrm{PI}) = \sum_{l\, m_l} \left[1 - \sum_{\gamma' l' m_l'} |S_{\gamma' l' m_l', \gamma l m_l}|^2 \right]. \tag{33}$$

F. Benchmarking

Cross sections from our model were benchmarked against and agreed with the results in [20], which is the most recent and accurate close-coupled model of He* collisions. We are not aware of any equivalent $B > 0$ cross section data that could be used as a benchmark. However, to include the magnetic interaction in our model we only had to add the (relatively straightforward) Zeeman term to the Hamiltonian. The code representing that term was checked for correctness.

G. Resonance search

Elastic and ionization cross sections are calculated at constant collisional energy over a grid of magnetic fields ranging from 0 to 10^4 G (0 to 1 T). A maximum grid spacing of 400 G is used to observe the broad behavior and identify resonances, with smaller grid spacing used around features of interest and where resonances were predicted in [18].

For each isotopic mixture we consider the two most experimentally relevant scattering channels, which are the two channels with lowest energy (under the hyperfine and Zeeman interactions). In bosonic He* the lowest energy channel corresponds to spin polarized atoms in the $m_f = +1$ state; this channel is the most experimentally accessible because the polarization minimises Penning ionization [32]. We do not expect resonances in the lowest energy fermionic channel as that channel involves identical fermions. However, we consider resonances in the second lowest energy fermionic channel, which can be experimentally accessed for example by using a radio-frequency sweep to transfer atoms from the lowest energy $|f, m_f\rangle = |3/2, 3/2\rangle$ state to the $|3/2, 1/2\rangle$ state before collision.

From the elastic scattering cross sections we calculate resonance locations and widths, by fitting Fano profiles to the data according to the equation:

$$\sigma_{\mathrm{el}}^{\mathrm{Fano}}(B) = \sigma_0 \frac{\left(q\frac{\Delta}{2} + B - B_0\right)^2}{\left(\frac{\Delta}{2}\right)^2 + (B - B_0)^2}. \tag{34}$$

Here σ_0 is the nonresonant background cross section, B_0 is the resonance location, q is a shape parameter, and Δ is the resonance width.

TABLE I. Identified resonance positions B_0 and widths Δ. Scattering channels are labeled in order of their energy: A and B respectively correspond to the lowest and second-lowest energy collision channels. In ^{4}He* the A channel corresponds to spin polarized atoms in the $m_f = +1$ state. When ^{3}He* atoms are involved the channels are linear combinations of different hyperfine states. Uncertainties are fitting uncertainties.

Mixture	Scattering channel	B_0 (G)	Δ (G)[b]
44	A	345.3(1)[a]	
	A	4881.09(2)	0.05(1)
	A	9752.98(3)	
34	A	129.99(5)[a]	
	A	4749.99(6)	
	A	9550(1)	
33	B	17598.06(3)	0.05(2)

[a]Resonance observable only when ionization is switched off.
[b]Widths are not given where the fit to the Fano profile produced errors greater than the widths themselves.

Because the Zeeman and hyperfine terms vary between the channels, total energy is not a good quantity to keep constant when comparing the scattering cross sections of different channels. Instead we compared cross sections at constant collisional wave number k_a (25). We performed all of our calculations at $k_a = 10^{-4}\, a_0^{-1}$. For ^{4}He* scattering at $B = 0$, this corresponds to energies $\sim 10^{-12}\, E_h$ or temperatures $\sim 1\ \mu$K.

We included all terms in the basis up to $l \leqslant 4$, which meant 120 states in 4-4 scattering, 450 in 3-4 scattering, and 435 in 3-3 scattering. We experimented with larger bases but found that $l_{\max} = 4$ was sufficient such that it was not the limiting factor in our calculations.

III. RESULTS AND DISCUSSION

Seven resonances identified in this study are described in Table I. Three each are identified in the lowest energy scattering channels of heteronuclear and bosonic collisions. Another resonance is identified in the second-lowest energy scattering channel of fermionic collisions. In this discussion we compare with the results of [18], which is the only existing theoretical study of He* Feshbach resonances.

In this work we have taken the uncertainty in resonance position as fitting uncertainties. However, there are other sources of error in the model itself, chiefly from the Born-Oppenheimer potentials. It is difficult to estimate the uncertainty in the model that comes from those potentials. To make such an estimate, extensive calculations would need to be repeated over a range of perturbations to the potentials. Estimating uncertainty due to potentials is an area where perturbative modeling techniques are better suited than close coupling.

Two of the three resonances identified in homonuclear ^{4}He* collisions (rightmost two resonances in Fig. 1) roughly coincide with the previous theoretical study. The resonance at 345 G is located within the range of previously forecast locations, which was 99 to 460 G [18]. This resonance has been searched for experimentally but was not observed [19]. However, the resonance is only visible when ionization is switched

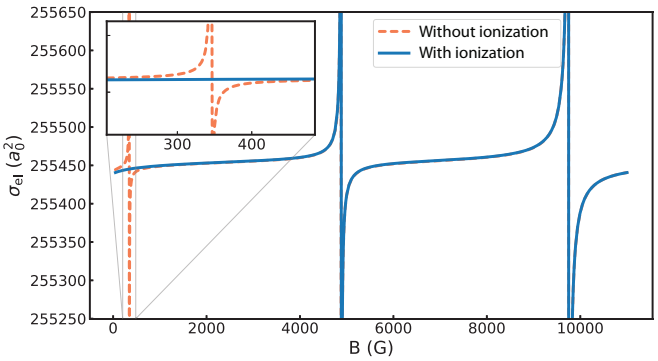

FIG. 1. Elastic cross section of bosonic ^{4}He* - ^{4}He* collisions in the lowest energy scattering channel. The blue solid line shows cross sections with Penning ionization accounted for; the orange dashed line shows cross sections with Penning ionization neglected. The orange dashed line lies under the blue solid line except for the first resonance.

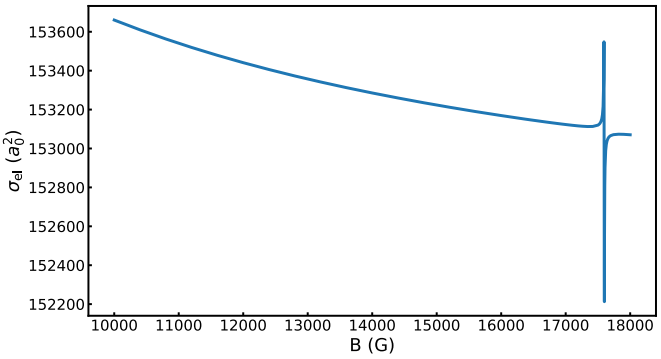

FIG. 2. Elastic cross section of fermionic ^{3}He* - ^{3}He* collisions in the second-lowest energy scattering channel. A single Feshbach resonance is identified near 17 600 G. This scattering channel is a linear combination of states where spin polarised atoms collide with unpolarized atoms of $m_f = -1/2$.

off in our model (orange line in Fig. 1). Our results indicate that it is broadened massively by ionization processes, which were neglected in the prior study.

We performed single-channel calculations of bound state energies via counting wave-function nodes [33] and matched the 345 G resonance to a bound state in the $|S = 0\rangle$ channel, in agreement with [18]. The Penning and autoionization processes are strong at short range for the singlet and triplet configurations, so those channels have much larger ionization cross sections than the quintet channel. This means resonances involving bound states in singlet and triplet channels have shortened lifetimes and commensurately broadened energy-space profiles. This is also why some resonances remain unchanged when ionization is included in the calculation: those resonances involve bound states in quintet channels, which may only ionize after a spin flip to the singlet or triplet configurations, causing ionization in those channels to be energetically suppressed. These results offer a complete explanation of the discrepancy between theory and experiment regarding the 345 G resonance.

We believe the resonance seen at 4881 G in Fig. 1 is the same as a previously predicted resonance at 5460 G [18]. Single-channel calculations of bound state energies via counting of wave function nodes [33], performed using this model, matched the resonance seen here to the same associated bound state as in that prediction. The third resonance at 9753 G was not previously predicted; however, its appearance is unsurprising. The 4881 G resonance is caused by coupling between the $|S = 2, m_S = +2\rangle$ scattering channel and a bound state in the $|S = 2, m_S = 0\rangle$ closed channel; however, that scattering channel may also couple to a bound state in the $|S = 2, m_S = +1\rangle$ channel. Because the Zeeman potential is directly proportional to the spin projection, when the spin projection between the channels is halved, the resonance condition for the same bound state:

$$\frac{-g_S\mu_B}{\hbar}B_0(m_{S_{\text{scat}}} - m_{S_{\text{bound}}}) = E_{\text{bound}} - \frac{\hbar^2k^2}{2\mu}, \qquad (35)$$

occurs at twice the magnetic field. Indeed, 9753 G is within 0.1% of 2×4882 G.

The fermionic Feshbach resonance seen in Fig. 2 was predicted previously [18], with our calculated value at the upper bound of the previously predicted range of values. Those previous bounds were determined by variation in the $S = 1$ potential.

The heteronuclear A channel resonance structure (Fig. 3) is qualitatively very similar to the bosonic A channel structure. This could be due to the independence of some of the coupling in the system from isotopic details of the constituent species. Both of the larger two heteronuclear resonances were previously predicted to exist [18]. Interestingly, the resonance centred at 9550 G was predicted to be narrower than the 4750 G resonance, but in these results resonance widths increase as B_0 increases. As with the small bosonic resonance, the ionization process broadens the 130 G resonance to the extent that it cannot be seen.

No Fano profiles were observed in the heteronuclear B channel (Fig. 4), including a very wide resonance previously predicted at 1214 G. Three other resonances in this channel were previously predicted, but without resonance widths

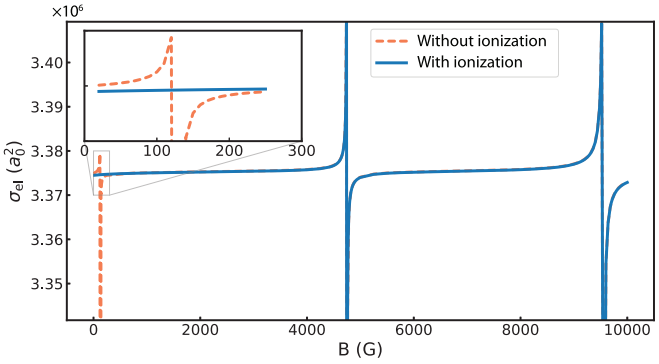

FIG. 3. Elastic cross section of heteronuclear ^{3}He* - ^{4}He* collisions in the lowest energy scattering channel. Blue solid lines show cross sections with Penning ionization accounted for; orange dashed lines show cross sections with Penning ionization neglected. Inset: one of the resonances is only visible when ionization is discounted from the model. The orange dashed line lies under the blue solid line except near the location of the first resonance.

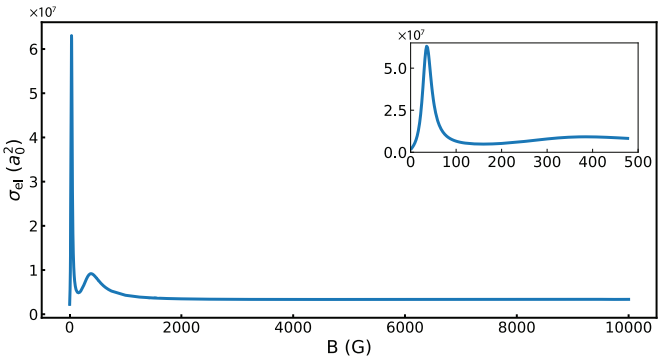

FIG. 4. Elastic cross section of heteronuclear ^{3}He* - ^{4}He* collisions in the second-lowest energy scattering channel. Inset: while no Fano profiles indicative of Feshbach resonances are identified, the cross section varies by over an order of magnitude across an experimentally accessible range of magnetic fields weaker than 100 G.

[18]. We thoroughly searched for a resonance predicted at 3618(6) G, scanning from 3598 to 3638 G with a grid spacing of 1 G; however, no field dependence was identified in the cross section.

Perhaps more interestingly, Fig. 4 shows that in this scattering channel there are variations in the elastic cross section that are inconsistent with a Fano profile. Similar curves appear in the ionization cross sections (not shown). The sharp spike in cross section at ∼35 G, reminiscent of a shape resonance [34], is particularly interesting, with the elastic cross section there varying by over an order of magnitude. While relatively large compared to the background, additional calculations at lower collisional energies (down to $k = 10^{-7}\, a_0^{-1}$) show that the feature is not a resonance: the scattering length does not diverge.

Unfortunately, our results do not identify a Feshbach resonance that appears experimentally useful. In the bosonic A channel ionization processes broaden the 345 G resonance to the point of insignificance. The resonance at 4881 G would likely pose difficulties in an experiment, as its location and width would demand a very powerful but stable electromagnet; these difficulties are magnified for the 9550 G resonance. This state of affairs also describes the heteronuclear A channel where the resonance structure is similar. The singular resonance in the fermionic B channel occurs at a larger magnetic field and is therefore even less useful.

In contrast to the identified (unbroadened) Feshbach resonances, the non-Feshbach variation in the 3-4 B channel cross section occurs over a range of magnetic field strengths (0–100 G) that is readily accessible in typical cold atom experiments. Because this variation is not a Feshbach resonance the scattering length does not diverge. However, with the elastic cross section varying by a factor of 30, by $\sigma = 4\pi a^2$ this would imply the scattering length varies by a factor of 5. This is a significant variation, and could be used in experiments such as many-body lattice physics [2] and interaction induced quantum phase transitions [3]. Because this channel is not between atoms in the lowest state (in which He* quantum gases are usually prepared, to minimize Penning ionization during cooling [7]) it would require one species of the He* atoms to be transferred between spin states, which could be achieved via, for example, an RF sweep. The lack of spin suppression following this sweep would likely cause ionization to be a practical hindrance, as our model calculates the ionization cross section for 3-4 B channel collisions to be 10^7 times larger than for spin polarized bosonic helium.

IV. CONCLUSION

We developed a close coupled model of ultracold He* atom collisions in the presence of a magnetic field and used it to search for Feshbach resonances. Several resonances were identified across bosonic, fermionic, and heteronuclear scattering channels; however, none are likely to be experimentally accessible. We identified that a predicted Feshbach resonance that was not seen in experiment is actually broadened by ionization processes. We also identified magnetic field dependence in the cross section of the second-lowest energy heteronuclear scattering channel, which, although not a Feshbach resonance, occurs at low magnetic fields that may be experimentally accessible.

ACKNOWLEDGMENTS

The authors would like to thank James Sullivan for helpful discussions and Andrew Truscott for careful reading of the manuscript. This work was supported through Australian Research Council (ARC) Discovery Project grant DP190103021. D.G.C. was supported by ARC Discovery Early Career Researcher Award No. DE170101024.

[1] M. H. Anderson, J. R. Ensher, M. R. Matthews, C. E. Wieman, and E. A. Cornell, Observation of Bose-Einstein condensation in a dilute atomic vapor, Science **269**, 198 (1995).

[2] I. Bloch, J. Dalibard, and W. Zwerger, Many-body physics with ultracold gases, Rev. Mod. Phys. **80**, 885 (2008).

[3] M. W. J. Romans, R. A. Duine, S. Sachdev, and H. T. C. Stoof, Quantum Phase Transition in an Atomic Bose Gas with a Feshbach Resonance, Phys. Rev. Lett. **93**, 020405 (2004).

[4] I. Bloch, J. Dalibard, and S. Nascimbène, Quantum simulations with ultracold quantum gases, Nat. Phys. **8**, 267 (2012).

[5] S. Braun, J. P. Ronzheimer, M. Schreiber, S. S. Hodgman, T. Rom, I. Bloch, and U. Schneider, Negative absolute temperature for motional degrees of freedom, Science **339**, 52 (2013).

[6] E. A. Donley, N. R. Claussen, S. L. Cornish, J. L. Roberts, E. A. Cornell, and C. E. Wieman, Dynamics of collapsing and exploding Bose–Einstein condensates, Nature (London) **412**, 295 (2001).

[7] W. Vassen, C. Cohen-Tannoudji, M. Leduc, D. Boiron, C. I. Westbrook, A. Truscott, K. Baldwin, G. Birkl, P. Cancio, and M. Trippenbach, Cold and trapped metastable noble gases, Rev. Mod. Phys. **84**, 175 (2012).

[8] S. S. Hodgman, R. G. Dall, L. J. Byron, K. G. H. Baldwin, S. J. Buckman, and A. G. Truscott, Metastable Helium: A New Determination of the Longest Atomic Excited-State Lifetime, Phys. Rev. Lett. **103**, 053002 (2009).

[9] D. C. Morton, Q. Wu, and G. W. F. Drake, Energy levels for the stable isotopes of atomic helium (4He I and 3He I), Can. J. Phys. **84**, 83 (2006).

[10] T. Jeltes, J. M. McNamara, W. Hogervorst, W. Vassen, V. Krachmalnicoff, M. Schellekens, A. Perrin, H. Chang, D. Boiron, A. Aspect, and C. I. Westbrook, Comparison of the Hanbury Brown–Twiss effect for bosons and fermions, Nature (London) **445**, 402 (2007).

[11] D. K. Shin, B. M. Henson, S. S. Hodgman, T. Wasak, J. Chwedeńczuk, and A. G. Truscott, Bell correlations between spatially separated pairs of atoms, Nat. Commun. **10**, 4447 (2019).

[12] P. Dussarrat, M. Perrier, A. Imanaliev, R. Lopes, A. Aspect, M. Cheneau, D. Boiron, and C. I. Westbrook, Two-Particle Four-Mode Interferometer for Atoms, Phys. Rev. Lett. **119**, 173202 (2017).

[13] S. S. Hodgman, W. Bu, S. B. Mann, R. I. Khakimov, and A. G. Truscott, Higher-Order Quantum Ghost Imaging with Ultracold Atoms, Phys. Rev. Lett. **122**, 233601 (2019).

[14] A. Perrin, H. Chang, V. Krachmalnicoff, M. Schellekens, D. Boiron, A. Aspect, and C. I. Westbrook, Observation of Atom Pairs in Spontaneous Four-Wave Mixing of Two Colliding Bose-Einstein Condensates, Phys. Rev. Lett. **99**, 150405 (2007).

[15] H. Cayla, S. Butera, C. Carcy, A. Tenart, G. Hercé, M. Mancini, A. Aspect, I. Carusotto, and D. Clément, Hanbury Brown and Twiss Bunching of Phonons and of the Quantum Depletion in an Interacting Bose Gas, Phys. Rev. Lett. **125**, 165301 (2020).

[16] R. Chang, Q. Bouton, H. Cayla, C. Qu, A. Aspect, C. I. Westbrook, and D. Clément, Momentum-Resolved Observation of Thermal and Quantum Depletion in a Bose Gas, Phys. Rev. Lett. **117**, 235303 (2016).

[17] J. A. Ross, P. Deuar, D. K. Shin, K. F. Thomas, B. M. Henson, S. S. Hodgman, and A. G. Truscott, Survival of the quantum depletion of a condensate after release from a harmonic trap in theory and experiment, arXiv:2103.15283.

[18] M. R. Goosen, T. G. Tiecke, W. Vassen, and S. J. J. M. F. Kokkelmans, Feshbach resonances in ^{3}He*-^{4}He* mixtures, Phys. Rev. A **82**, 042713 (2010).

[19] J. S. Borbely, R. van Rooif, S. Knoop, and W. Vassen, Magnetic-field-dependent trap loss of ultracold metastable helium, Phys. Rev. A **85**, 022706 (2012).

[20] D. G. Cocks, I. B. Whittingham, and G. Peach, Ultracold homonuclear and heteronuclear collisions in metastable helium, Phys. Rev. A **99**, 062712 (2019).

[21] J. Bezanson, A. Edelman, S. Karpinski, and V. B. Shah, Julia: A fresh approach to numerical computing, SIAM Rev. **59**, 65 (2017).

[22] C. Rackauckas and Q. Nie, Differential equations.jl – A performant and feature-rich ecosystem for solving differential equations in Julia, J. Open Res. Software **5**, 15 (2017).

[23] H. T. C. Stoof, J. M. V. A. Koelman, and B. J. Verhaar, Spin-exchange and dipole relaxation rates in atomic hydrogen: Rigorous and simplified calculations, Phys. Rev. B **38**, 4688 (1988).

[24] M. Przybytek and B. Jeziorski, Bounds for the scattering length of spin-polarized helium from high-accuracy electronic structure calculations, J. Chem. Phys. **123**, 134315 (2005).

[25] M. W. Müller, A. Merz, M. W. Ruf, H. Hotop, W. Meyer, and M. Movre, Experimental and theoretical studies of the Bi-excited collision systems He*(2^3S) + He*(2^3S, 2^1S) at thermal and subthermal kinetic energies, Z. Phys. D **21**, 89 (1991).

[26] T. J. Beams, G. Peach, and I. B. Whittingham, Spin-dipole-induced lifetime of the least-bound $^5\Sigma_g^+$ state of He(2^3S_1) + He(2^3S_1), Phys. Rev. A **74**, 014702 (2006).

[27] C. W. Drake, Magnetic Moment of Helium in Its $^3S_1$ Metastable state, Phys. Rev. **112**, 1627 (1958).

[28] J. L. Flowers, B. W. Petley, and M. G. Richards, A Measurement of the nuclear magnetic moment of the helium-3 atom in terms of that of the proton, Metrologia **30**, 75 (1993).

[29] S. D. Rosner and F. M. Pipkin, Hyperfine structure of the 2 $^3S_1$ State of He^3, Phys. Rev. A **1**, 571 (1970).

[30] B. J. Garrison, W. H. Miller, and H. F. Schaefer, Penning and associative ionization of triplet metastable helium atoms, J. Chem. Phys. **59**, 3193 (1973).

[31] F. H. Mies, A scattering theory of diatomic molecules: General formalism using the channel state representation, Mol. Phys. **41**, 953 (1980).

[32] G. V. Shlyapnikov, J. T. M. Walraven, U. M. Rahmanov, and M. W. Reynolds, Decay Kinetics and Bose Condensation in a Gas of Spin-Polarized Triplet Helium, Phys. Rev. Lett. **73**, 3247 (1994).

[33] A. Messiah, *Quantum Mechanics* (Dover, Mineola, NY, 1999).

[34] C. J. Joachain, *Quantum Collision Theory* (North-Holland, Amsterdam, 1975).